The Astrophysical Journal, 954:117 (12pp), 2023 September 10 https://doi.org/10.3847/1538-4357/ace163

Slowly Rotating Accretion Flow Around Supermassive Black Holes in Elliptical Galaxies: Case With Outflow

Razieh Ranjbar and Shahram Abbassi
Department of Physics, Faculty of Science, Ferdowsi University of Mashhad, Mashhad, Iran; razieh.ranjbar@mail.um.ac.ir, abbassi@um.ac.ir
Received 2023 March 15; revised 2023 June 21; accepted 2023 June 22; published 2023 August 28

Abstract

Observational evidence and many numerical simulations show the existence of winds (i.e., uncollimated outflows) in the accretion systems of elliptical galaxy centers. One of the primary aims of this study is to investigate the solutions of slowly rotating accretion flows around supermassive black holes with outflows. This paper presents two distinct physical regions, supersonic and subsonic, which extend from the outer boundary to the black hole. In our numerical solution, the outer boundary is chosen beyond the Bondi radius. Due to strong gravity, we ignore outflow (i.e., $s = 0$) in the inner region (within $\sim 10 r_s$). The radial velocity of the flow at the outer region is significantly increased due to the presence of the outflow. Compared to previous works, the accretion mode, namely, the slowly rotating case, that corresponds to low accretion rates that have general wind output is carefully described, and the effect of the galaxy potential and feedback by the wind in this mode are taken into account. As the power-law form of the mass accretion rate is mathematically compatible with our equations, we consider a radius-dependent mass accretion rate ($\dot{M}_{\rm in} \propto r^s$), where s is a free parameter and shows the intensity of outflow. There is an unknown mechanism for removing the mass, angular momentum, and energy by outflows in this study. The effects of the outflow appear well on the outer edge of the flow.

Unified Astronomy Thesaurus concepts: Elliptical galaxies (456); Accretion (14)

1. Introduction

The majority of cool-core clusters have massive black holes (BHs) in their central regions, which produce persistent relativistic jets. It is important to point out that these jets are highly interactive with the ambient medium, and they inject a large amount of energy into the surrounding gas, which is key to AGN feedback. M87 is a supergiant elliptical galaxy near the center of the Virgo cluster that serves as a unique laboratory for studying AGN jets and their formation and acceleration thanks to its proximity at a distance of 16.7 Mpc and its extremely massive black hole of mass $M_{\rm BH} = (3.5\text{–}6.6) \times 10^9 M_\odot$ (Luc-chini et al. 2019). Active galactic nuclei (AGNs) feedback plays a crucial role in the evolution of the host galaxy (Fabian 2012; King & Pounds 2015). Over the past 20 yr, there has been tremendous growth in the literature related to AGN feedback (Harrison et al. 2018). The outputs of the AGNs, such as radiation, wind, and jet, interact with the interstellar medium (ISM) in the host galaxy and change the density and temperature of the ISM. It follows that star formation activity will be affected, and accordingly galaxy evolution will be affected as well. For evaluating the effects of AGN feedback, the value of the accretion rate and the model of accretion physics play a critical role as they determine the magnitude of the AGN output.

In order to study AGN feedback, one of the most important quantities is the mass accretion rate of the BH, which has a great deal to do with AGN power. There is a widely held belief that much of the energy behind astronomical objects is due to mass accretion onto black holes, as seen in AGNs, X-ray binaries, and even gamma-ray bursts (Frank et al. 2002). It may be appropriate to use the spherical Bondi model to describe galaxy evolution as the central AGN is often found in the region with the densest atmosphere within the cluster (Bondi 1952; Baganoff et al. 2003; Di Matteo et al. 2003). AGNs can receive sufficient fuel from the Bondi accretion rate based on Chandra's observations of M87 (Di Matteo et al. 2003). In addition, the Bondi model is an affordable option for modeling hot accretion flows. The Bondi model is undoubtedly one of the best transonic models available today. However, a spherically symmetric Bondi accretion cannot occur in nature and black hole accretion processes are almost always associated with rotating gas flows, so a modified Bondi model is needed. Narayan & Fabian (2011), hereafter NF11, discussed low-angular-momentum accretion and added a slow rotation to Bondi accretion flows. As an intermediate case between Bondi and advection-dominated accretion flows (ADAFs), this model was applied to Sgr A* and M87. In recent years, Bondi solutions and slowly rotating accretion flows have been developed by taking galaxy gravitational potential into account (Ranjbar et al. 2022 hereafter R22; Korol et al. 2016; Ciotti & Pellegrini 2017, 2018; Samadi et al. 2019). Early analytical work assumed that mass accretion rates were independent of the radius, $\dot{M}(r) =$ constant, so in this case, radial density profiles satisfy $\rho \propto r^{-3/2}$ (e.g., Narayan & Yi 1994). The dynamics of the accretion flow have been studied extensively in hydrodynamic (HD) and magnetohydrodynamic (MHD) numerical simulations (e.g., Stone et al. 1999; Igumenshchev et al. 2000; Proga & Mitchell 2003; McKinney et al. 2012). Sgr A* and NGC 3115 are two of the best targets of Chandra's observations that show flat density profiles with $\rho \propto r^{-1}$ inside the Bondi radius (Wang et al. 2013). Regarding recent numerical simulations, only a fraction of the Bondi rate is able to reach the supermassive black hole (SMBH) due to outflows originating from the accretion flow (e.g., Yuan et al. 2012; Li et al. 2013). It seems that objects created by accretion,

such as galaxies and stars, have generated outflows that have significantly impacted the surrounding environment. There is also a belief that the outflow plays a more significant role in suppressing star formation and the BH accretion rate (Yuan et al. 2018). It is therefore worthwhile to consider outflows in Bondi-like accretion flow physics.

Recent observations and simulations suggest that outflows/winds play a significant role in accretion systems. One of the most important findings in recent years in hot accretion flows has been the discovery of the strong outflow/wind that originates from the accretion flow (Narayan et al. 2012; Yuan et al. 2012; Li et al. 2013). Due to the highly ionized nature and absence of an absorption line of a hot accretion flow, it is difficult for us to observe wind directly from it (Bu & Yang 2019). The presence of wind in hot accretion flows is evident from indirect observations. Observation of the 3 million seconds of Chandra from the SMBH in the center of our galaxy, Sgr A*, confirmed this theoretical prediction recently (Wang et al. 2013). It is interesting to find that wind is not only a key factor in accretion physics but also plays a significant role in the feedback of AGNs as well (e.g., Ostriker et al. 2010; Gan et al. 2014). Observations of low-luminosity AGNs (LLAGNs; e.g., Crenshaw & Kraemer 2012; Wang et al. 2013; Cheung et al. 2016), as well as black hole X-ray binaries (Homan et al. 2016), have shown that hot accretion flows are influenced by winds. Also, the existence of outflows in radiatively inefficient accretion flows is confirmed by many observations (e.g., Wang et al. 2013; Ma et al. 2019; Muñoz-Darias et al. 2019). Therefore, the numerical simulation result is confirmed by observations. In accordance with numerical simulations and analytical models of the hot accretion flow, the accretion rate decreases with decreasing radius, so most of the gas is lost between the Bondi radius and the event horizon (e.g., Igumenshchev & Abramowicz 1999; Stone et al. 1999; Yuan & Bu 2010; Begelman 2012). Many analytical models have been developed in recent years to investigate how hydrodynamical winds affect the structure of advection-dominated accretion flows (Abbassi et al. 2010; Mosallanezhad et al. 2014; Ghasemnezhad & Abbassi 2016). The outflow is particularly crucial as it carries mass, momentum, and energy to the surrounding environment, exerting significant influence there (Botella et al. 2022; Hu et al. 2022). Winds are believed to play a crucial role in the interaction between AGNs and their host galaxies (e.g., Ciotti et al. 2010; Ostriker et al. 2010; Weinberger et al. 2016; Ciotti et al. 2017; Hu et al. 2022).

NF11 studied the slowly rotating accretion flow in the region very close to the black hole, from r_s (where r_s is the Schwarzschild radius) to the region beyond the Bondi radius. We recalculate the NF11 solutions for accretion flow with small angular momentum by including outflow effects. We find that the real accretion rate onto the black hole significantly deviates from the value calculated by NF11. In this paper, we study the slowly rotating accretion flow in the region from 0.01 of r_s to the outer boundary. The outer boundary is quite large, almost 3 times larger than the Bondi radius. This paper differs from that of NF11 in two aspects. First, in NF11, only the black hole gravity is taken into account. However, in the region around 10 parsec, the gravitational force of a nuclear star is comparable to that of the central black hole. The star's gravity may be important and needs to be considered. In the present paper, we will take the gravitational potential of the galaxy's stars into account. Second, in NF11, the effect of outflows and significant radial exchanges of energy are suppressed. The mass conservation, Equation (1) of NF11, explicitly ignores such outflows. In the present work, we solve differential equations in the presence of an outflow. A general mechanism for producing outflows is considered instead of a detailed description of power outflow mechanisms. The presence of an outflow is beneficial to study the effect of AGN feedback on galaxy formation and evolution. It is complex to consider the interactions between the outflowing energy, mass, and momentum with the ambient fluids, and we postpone this discussion to the next article in the series. The rest of the paper is planned accordingly. Section 3.1 compares our results with those of BY19, and also, we consider the thickness of flow ($H \neq r$) and investigate how outflows affect the thickness. Finally, we investigate the AGN feedback by calculating the energy and momentum fluxes of the outflow and compare it to the previous work of Yuan et al. (2018). In this paper, we focus on the case without a magnetic field and convection. The paper is organized as follows.

In Section 2, we analyze the basic equations, and various boundary conditions and explain our numerical method. The results of the numerical solution are given in Section 3, and finally, in Section 4, we summarize our results.

2. Model

2.1. The Structure of the Accretion Flow in Presence of an Outflow

In this study, we consider slowly rotating, steady, viscous accretion flows onto a nonrotating SMBH by including the role of outflows, which are commonly referred to as hot accretion flows. Such flows are nearly spherical, so the height-integrated differential equations can describe them well. In order to simplify our model, we assume all the variables are functions only of the radius and independent of time. Under these assumptions, we can obtain the basic conservation equations. In the presence of an outflow, the continuity equation of the accretion flow is

$$\frac{d}{dr}(4\pi r^2 \rho v) + \frac{d\dot{M}_{\rm w}}{dr} = 0, \tag{1}$$

where ρ is the density of the gas, v is the radial inflow velocity of gas ($v < 0$), and $\dot{M}_{\rm w}$ is the mass-loss rate owing to the outflow. It can be concluded that the mass accretion rate varies with the radius according to this equation.

The mass-loss rate $\dot{M}_{\rm w}$ is adopted from Knigge (1999; hereafter K99):

$$\dot{M}_{\rm w}(R) = \int_{r_c}^{r} \dot{m}_{\rm w}(r) dr, \tag{2}$$

where r_c denotes the sonic point radius, and $\dot{m}_w$ is the mass-loss rate per unit area from each flow face. Whenever mass is carried away by outflow, the mass accretion rate decreases inward. The mass accretion rate is expressed using the power-law form for several reasons below. The first benefit is that it makes solving differential equations simple. On the other hand, all wind launching mechanisms can be described with the K99 wind model, which is a general and parametric model. Lastly, the power-law form is mathematically compatible with our governing differential equations. We adopt the power-low form

for $\dot{M}_{\rm in}$ as follows

$$\dot{M}_{\rm in} = -4\pi r^2 \rho v = \dot{M}_{\rm out}\left(\frac{r}{r_{\rm out}}\right)^s, \quad for \quad r_{\rm c} < r < r_{\rm out}, \quad (3)$$

where s is the mass-loss power-law index and represents the strength of the outflow. Also, $r_{\rm out}$ and $\dot{M}_{\rm out}$ are the radius and the mass accretion rate in the outer boundary, respectively. A simulation paper by Ohsuga et al. (2005) demonstrates that s is not a constant in the flow, but its average value can be approximated around 1 (Kumar & Gu 2018). The analytical approach has limitations, so we considered s as a constant and a parameter in a particular solution ($0 < s < 1$). The mass accretion rate at the black hole horizon is

$$\dot{M}_{\rm BH} = \dot{M}_{\rm out}\left(\frac{r_{\rm c}}{r_{\rm out}}\right)^s. \quad (4)$$

In this work, we assume $\dot{M}_{\rm BH}$ equal to $\dot{M}_{\rm c}$, the mass accretion rate in the sonic point. Actually, the power-law variation in $\dot{M}_{\rm in}$ with r is not likely to continue all the way down to r_s, and it will probably cease somewhere near $r_{\rm in}$ on the order of $10r_s$ (or even tens of r_s; Yuan & Narayan 2014). As in the present study, the sonic radius is constrained to approximately $10r_s$, we assume that the power-law variation in $\dot{M}_{\rm in}$ will continue to $r_{\rm c}$. With the integration of Equation (1), the mass flux of outflow gives

$$(r) = \dot{M}_{\rm in}(r) - \dot{M}_{\rm BH}. \quad (5)$$

The second term of the right side is the net mass accretion rate that is accreted into the SMBH. According to Equation (5), we have:

$$d\dot{M}_{\rm in}/dr = d\dot{M}_{\rm w}/dr. \quad (6)$$

On the other hand, it has been found that the gravitational influence of the galaxy's stars should not be ignored at the parsec scale (Bu et al. 2016; Yang & Bu 2018). In calculating the total gravity, we consider the gravitational force of the stars in the galaxy as our computational scale covers subparsec and parsec scales. The total gravitational potential is as follows:

$$\Phi = \phi_{\rm BH} + \phi_{\rm galaxy}, \quad (7)$$

where $\phi_{\rm BH}$ is the potential of a black hole to emulate the general relativistic effects of a Schwarzschild black hole. We use the gravitational potential by Paczynsky & Wiita (1980),

$$\phi_{\rm BH} = -\frac{GM}{r - r_{\rm s}}, \quad (8)$$

where M is the mass, and $r_{\rm s} \equiv 2GM/c^2 = 2r_{\rm g}$ denotes the Schwarzschild radius of the nonrotating black hole. The self-gravity of the accretion flow is neglected, and $\phi_{\rm galaxy}$ is the galaxy potential,

$$\phi_{\rm galaxy} = \sigma^2 \ln r + C, \quad (9)$$

where C is a constant, and σ is the dispersion velocity of stars (Bu et al. 2016). It is common for elliptical galaxies with a central black hole mass $M_{\rm BH} = 10^8 M_\odot$ to have a stellar dispersion velocity of 150–250 km s^{-1}. Similarly to R22, we consider the velocity dispersion of stars to be a constant of the radius, which is $\sigma = 200$ km s^{-1} (Kormendy & Luis 2013).

The radial momentum equation is

$$v\frac{dv}{dr} = -(\Omega_{\rm K}^2 - \Omega^2)r - \frac{1}{\rho}\frac{d}{dr}(\rho c_{\rm s}^2) - \frac{\sigma^2}{r}, \quad (10)$$

where $\Omega_{\rm k}$ is the Keplerian angular velocity. We denote the isothermal sound speed by $c_{\rm s} = (P/\rho)^{1/2}$, and P is the total pressure of the gas.

In our model, it is assumed that matter ejected from the flow at radius r carries away specific angular momentum $(lr)^2\Omega$, where l is a dimensionless parameter representing the amount of angular momentum carried away by the outflow, and Ω is the angular velocity in the flow at radius r. Owing to the presence of the outflow, the angular momentum equation takes the form

$$\frac{d}{dr}(4\pi r^4 \rho \nu \Omega) = \frac{d}{dr}\left(4\pi\nu\rho r^4 \frac{d\Omega}{dr}\right) - (lr)^2\Omega\frac{d\dot{M}_{\rm w}}{dr}. \quad (11)$$

A value of $l = 0$ corresponds to a nonrotating outflow, which cannot extract angular momentum, and the flow only loses mass. $l > 0$ indicates outflowing materials that carry away angular momentum (Knigge 1999; Abbassi et al. 2013; Ghasemnezhad & Abbassi 2016; Habibi & Abbassi 2019). Furthermore, $0 < l < 1$ corresponds to a family of outflows that carry away less angular momentum than the outflow material had before leaving the accretion flow. Models with $l > 1$ also effectively describe centrifugally driven magnetic outflows, which can remove a large amount of angular momentum from the flow (Blandford & Payne 1982). We note that hydrodynamical outflows are in stark contrast to magnetically driven outflows, in which the gas may move along the field lines corotating with the flow to a distance far from the flow surface, and therefore a substantial fraction of the flow angular momentum may be removed through magnetically driven outflows (e.g., Lubow et al. 1994; Cao & Spruit 2002). In the second term on the right-hand side of Equation (11), the outflow provides an angular momentum sink. In this model, a simple approach can be applied to a wide range of outflow models (for more information, see K99), where ν is the kinematic coefficient of viscosity, which is defined by

$$\nu = \alpha c_{\rm s} r. \quad (12)$$

As mentioned in Shakura (1973), α is the viscosity parameter and is usually assumed to be a constant. Integrating Equation (11) yields

$$\frac{d\Omega}{dr} = \frac{v}{\alpha c_{\rm s} r^3}\left(\Omega r^2\left(1 - \frac{sl^2}{s + 1/2}\right) - j\right), \quad (13)$$

where the integration constant j represents the specific angular momentum per unit mass that is swallowed by the black hole.

The integral of angular momentum is a bit difficult to calculate. For simplicity, in this case, we utilize an approximate to derive Equation (13), which is $d\Omega/dr \propto -3\Omega/2r$. It is estimated that at $r = r_{\rm B}$, the most rapidly rotating solution ($L = 85$) has centrifugal support of only 10% Keplerian (NF11). The mass-loss rate has also been expressed in a power-law form. Eventually, the energy equation reads

$$\frac{2r\rho v}{(\gamma - 1)}\frac{dc_{\rm s}^2}{dr} - 2rc_{\rm s}^2 v\frac{d\rho}{dr} = 2r\rho f\nu r^2\left(\frac{d\Omega}{dr}\right)^2 - \frac{1}{2}\eta\dot{m}_{\rm w}v_{\rm k}^2. \quad (14)$$

The adiabatic index of the gas is γ, which, in our work, equals 5/3. η is a free and dimensionless parameter in our

model. In accordance with the energy loss owing to the outflow, parameter η may change (K99). In most cases, we are interested in a radiatively inefficient flow in which radiative cooling is negligible. Hence, the first term on the left-hand side of Equation (14) represents the viscous heating rate per unit volume, and the second term on the left-hand side of it is the energy losses owing to the outflow (K99). In order to measure the degree to which the flow is advective, we use parameter f (Narayan & Yi 1994). Generally, for radiative-cooling-dominated flows $f\sim 0$, such as standard thin disks or Shapiro-Lightman-Eardley disks, while for advection-dominated flows $f\sim 1$. Hence, in this paper, we assume that $f=1$ (full advection case). The approximation works well whenever radiative cooling is less than a few percent of the heating rate.

2.2. The Inner Region

A viscous, slowly rotating accretion flow with outflow is described by the equations in Section 2.1. In the region near the SMBH, accreting gas passes inside the sonic radius r_c and becomes supersonic. In some general relativistic simulations of hot accretion flows, Yuan et al. (2012), Bu et al. (2013), Sądowski et al. (2013), and Yuan et al. (2012) have shown that the accretion rate is constant within $\sim 10r_s$. This may be caused by the strong gravity around the black hole so $s=0$, which means that there is no mass loss from the flow. Also, in the inner regions, gravity is greater than the pressure force, and the radial velocity is considerably large (so the viscous timescale is short), which means that only a weak outflow can form (Stone et al. 1999; Wu et al. 2022). Furthermore, in regions very close to the SMBH, the timescale of outflow formation is more than the accretion timescale, so we may ignore the outflow effect in this region. Thus, we assume that outflows from inside $10r_s$ are quite weak. Certainly, the simplest description that one could propose would be to imagine that there is no energy, mass, or angular momentum transfer from the supersonic flow to the surrounding environment. Nonetheless, in the present work, we neglect viscosity α in the inner region following the similar argument given in NF11. Furthermore, it is important to note that the velocity dispersion of stars contributes significantly to the distribution of gravitational forces within the galaxy, especially when the radius exceeds 1 pc (Yang & Bu 2018; R22). This causes the gravitational effect of stars close to the black hole to greatly reduce or disappear completely. Hence, all of the differential equations become algebraic equations (see Section 2.2 of NF11 for more details).

2.3. Boundary Conditions

The accretion flow around the SMBH ultimately falls in the center; away from the SMBH, the flow is subsonic. These transonic flows are supersonic after passing the sonic radius and fall toward the BH with speeds near the speed of light. Because of this, our computational domain consists of two parts. The inner region is supersonic. The viscosity of the flow in this region is low, so we consider an inviscid flow and assume that the inner region has inflow only and ignore outflow here. The other region extends from the sonic radius to the outer boundary; in this region, we have viscous inflow/outflow fluid. The main differential equations consist of four variables. We need four boundary conditions to solve them properly. In addition, j is an eigenvalue, so we induced another constraint for adding one more boundary condition. On the other hand, the location of the sonic radius is unknown; thus, we require another boundary condition. This problem has six boundary conditions, similar to those in NF11.

Following the procedure adopted in previous works for studying transonic accretion flows around BH/compact objects (e.g., Chakrabarti 1996; Narayan et al. 1997; Mukhopadhyay & Ghosh 2003), we combine Equation (3) with differential Equations (10), (13), and (14), so the following relations form

$$\frac{d\ln v}{dr}=\frac{\mathcal{N}}{\mathcal{D}}, \tag{15}$$

$$\mathcal{N}=\frac{(\Omega_k^2-\Omega^2)r}{c_s^2}+\frac{\gamma(s-2)}{r}+\frac{(\gamma-1)\alpha r^3}{vc_s}\left(\frac{d\Omega}{dr}\right)^2 + (\gamma-1)\frac{\eta}{4}\frac{s}{rc_s^2}(r^2\Omega_k^2)+\frac{\sigma^2}{rc_s^2}, \tag{16}$$

$$\mathcal{D}=\gamma-\frac{v^2}{c_s^2}. \tag{17}$$

As the flow at the sonic radius must be smooth, this equation gives us two boundary conditions in $r=r_c$,

$$\gamma c_s^2-v^2=0, \tag{18}$$

$$(\Omega_k^2-\Omega^2)r_c+\gamma\left(\frac{(s-2)c_s^2}{r_c}+(\gamma-1)\frac{\eta}{4}\frac{s}{r_c}(r_c^2\Omega_k^2)\right) + \frac{(\gamma-1)\alpha r_c^3 c_s}{v}\left(\frac{d\Omega}{dr}\right)^2+\frac{\sigma^2}{r_c}=0. \tag{19}$$

The third boundary condition at the sonic radius is acquired from the angular momentum equation. As viscosity and outflow have been ignored in the supersonic region, one may consider that the specific angular momentum of the gas remains constant. Thus we have

$$\Omega r_c^2\left(1-\frac{l^2 s}{s+1/2}\right)-j+\frac{2\alpha c_s\Omega r_c^2}{v}=0. \tag{20}$$

The rest of the boundary conditions are in the outer boundary. In most astrophysical systems, the accretion geometry consists of two zones, the outer cold zone, as described by the thin disk model, and the inner hot zone, represented by the hot accretion mode. Previous studies have assumed that the flow begins in a state of a geometrically thin accretion disk (NKH97). However, in other cases like Sgr A* and M87, the gas is hot at the Bondi radius and remains hot up to the inner edge. The Bondi radius is generally considered the outer boundary of the accretion flow surrounding a SMBH (M87, Sgr A*), where the thermal energy of the external surroundings is equal to its potential energy due to the gravitational field of the black hole (Yuan & Narayan 2014).

In the Bondi or even slowly rotating solutions, the temperature and density at the outer boundary play a crucial role and may be used as outer boundary conditions. The temperature value at the outer boundary is adopted as 6.5×10^6 K, which corresponds to the observed values for the interstellar medium at the nucleus of an elliptical galaxy at the center of a cool-core group or cluster of galaxies (NF11).

Therefore, we have two conditions at the outer boundary

$$c_s = c_{out}, \quad r = r_{out}$$
$$\rho = \rho_{out}, \quad r = r_{out}. \tag{21}$$

There is no doubt that outflow causes the surrounding environment to heat up, and consequently, it further complicates the problem. For simplification, we assume that the temperature at the outer boundary remains constant without incorporating outflow effects. The temperature of the halo surrounding most large elliptical galaxies ranges between 1 and 10 million Kelvin (it is in the range of the virial temperature; Roshan & Abbassi 2014). Indeed, the present work is an attempt to provide a more thorough survey of solutions by adopting different values of the temperature in the outer boundaries. As suggested by NF11, our solutions are based on $T_{out} = 6.5 \times 10^6$ K. According to the intended temperature at the external medium, the speed of sound is equal to $c_{out} = 10^{-3}c$, and the density contractually is considered to be $\rho_{out} = 1$.

The last boundary condition that we need comes from the angular velocity in the external medium. We assume that the slowly rotating gas has constant angular velocity in the outer boundary and that the outflow has no effect on the surrounding gas.

$$\Omega = \Omega_{out}, \quad r = r_{out}. \tag{22}$$

The angular momentum of the gas is one of the most important physical quantities in rotating accretion flows. There is an open question regarding the amount and distribution of angular momentum in the accreting matter, but it is believed that models with low-angular-momentum content are the most promising (Yuan et al. 2002; Proga & Mitchell 2003; Czerny et al. 2007). We introduce a dimensionless special angular momentum equal to the ratio of the specific angular momentum of the external gas l_{out} to the specific angular momentum of the marginally stable orbit l_{ms}.

$$L = \frac{l_{out}}{l_{ms}}. \tag{23}$$

For the Paczynsky & Wiita potential, l_{ms} is

$$l_{ms} = \sqrt{\frac{27}{8}}\, c r_s. \tag{24}$$

3. Numerical Results

In this section, we describe the numerical results of slowly rotating accretion flows with outflows. The structure of a quasi-spherical accretion flow with outflow is drastically changed compared to the classical Bondi solution, and the mass accretion rate onto the BH is significantly reduced. The conventional value of $\gamma = 5/3$ is adopted in all our calculations. Also, all calculations are done with the viscosity parameter $\alpha = 0.1$, which is roughly in accordance with what is suggested by the numerical simulations of Bai & Stone (2013) and Bu & Yang (2019). We numerically solved the main set of equations using the relaxation method. The relaxation method is a powerful technique for differential equations with appropriate boundary conditions at the outer radius and the sonic point. We can obtain the global structure of the slowly rotating accretion flow in the presence of an outflow by integrating these differential equations from the outer boundary to the black hole horizon. The flow passes smoothly from the sonic point and falls into the black hole (for more details, see R22). The outer radius of the accretion flow $r_{out} = 3r_B$ is adopted. In the inner region, a set of algebraic equations describe the flow, which is easily solved. As discussed in Section 2, there is a set of inputs such as s, η, and l, which describe the outflow properties. Mass, energy, and angular momentum can be taken away by outflows, which generally reduces the mass accretion rate.

In Figure 1, the global solutions for the slowly rotating accretion flow have been illustrated by adopting various values of the mass-loss power-law index s. These figures show the distributions of the radial velocity, angular velocity, specific angular momentum, and density, respectively. In panel (a) of Figure 1, the radial velocity is plotted as a function of the radius with different values of s while $l = 1$ and $\eta = 1$. For comparison, the case without outflows has been plotted with solid black lines. The sonic radius r_c, shown by the black dots, is located almost close to the marginally stable orbit $r_{ms} = 3r_g$. Physically, the outflows are restrained in the inner regions by a strong gravitational force of the central black hole. This figure illustrates well how outflow affects the outer region. Panel (b) illustrates the variation in angular velocity as a function of the radius. The sloping dotted line in panel (b) shows the Keplerian angular velocity Ω_K while the solution with $s = 0$ is plotted as black lines. Panel (c) of Figure 1 shows the radial variation in the specific angular momentum of the accretion flow l_{flow}. The distribution of the Keplerian angular momentum $l_K = \Omega_K r^2$ is shown by the dotted line for comparison. Panel (d) shows the profile of density ρ for three solutions. Due to the fact that the mass accretion rate decreases with the radius, the density profile of the accretion flow becomes flatter than when the mass accretion rate is constant. Consequently, the density profile flattens compared to the work of NF11. These results have been strongly supported by observations in the case of Sgr A*(Yuan et al. 2003), the low-luminosity AGN NGC 3115 (Wong et al. 2011), and black holes in elliptical galaxies (Di Matteo et al. 2000). Unlike the old picture where the accretion rate posses a constant value, many hydrodynamics (HD) and magnetohydrodynamics (MHD) numerical simulations demonstrate clearly that the inflow accretion rate decreases with decreasing radius (Igumenshchev & Abramowicz 1999; Stone et al. 1999; Yuan et al. 2012, 2012; Samadi & Abbassi 2016). It is commonly accepted that this varying inflow rate is caused by a mass loss in a wind/outflow. In Figure 2, we plot the velocities of the accretion flows as functions of the radius with different values of s. It clearly shows that the radial velocity of the gas with outflow in the outer regions is significantly higher than for the case without outflow. According to Figure 2, the radial and azimuthal velocities are different when outflow is present or absent, especially in the subsonic region, where the outflow is more effective. The radial velocity in the inner part of the flow is not affected by the outflow, but the outer part is enhanced by the rotating outflow in comparison with the no outflow case (Abbassi et al. 2013). For a given set of parameters, the azimuthal velocity is fairly sub-Keplerian. As a comparison, we also plot the results without outflows in the same figures. The azimuthal velocity profiles are plotted as a function of the radius (solid violet line ($s = 0$) and yellow dashed line ($s = 0.2$)). It is clear that if the exponent s decreases, the flow will rotate more slowly than without outflows. In Figure 3, the mass accretion rates as functions of the radius are plotted for the global solutions for various values of exponent s. We compare our modified solutions with the global solution of the

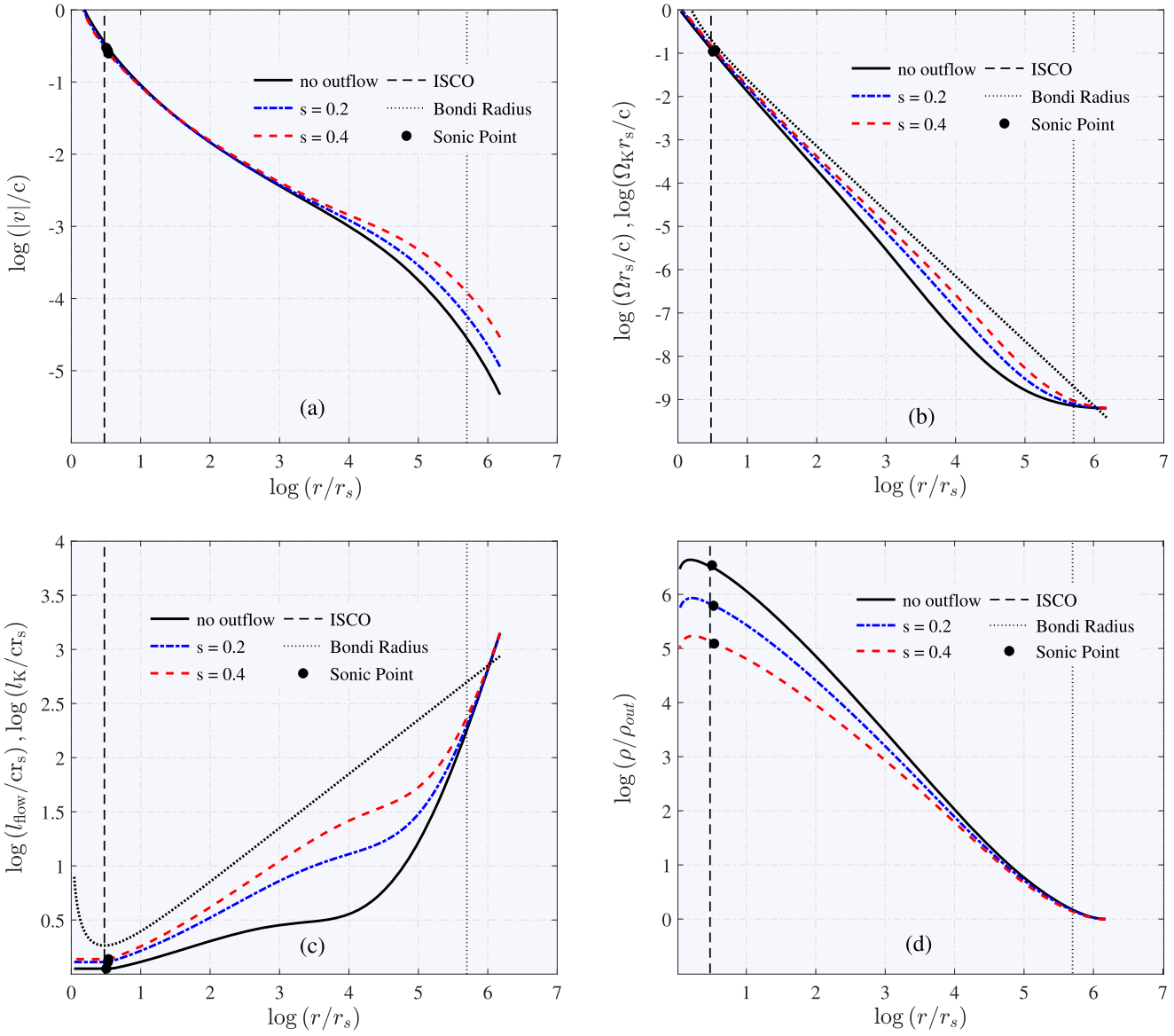

Figure 1. Global solutions for $L = 85$, $\alpha = 0.1$, $\gamma = 5/3$, and $T_{\rm out} = 6.5 \times 10^6$ K. The three solutions shown have (s, $r_{\rm c}$) = (0, 3.1981), (0.2, 3.3651), and (0.4, 3.4381), respectively. The position of the critical point is indicated by a solid dot (saddle). The dotted curves show the Keplerian angular momentum $\Omega_{\rm K}$ and the Keplerian specific angular momentum $l_{\rm K} = \Omega_{\rm K} r^2$. Variations in the flow variables with the radius r are seen in all four panels. Panel (a): variation in the radial velocity of the accretion flow with the radius. Panel (b): radial variation in the angular momentum Ω in the three solutions. Panel (c): specific angular momentum of the accretion flow $l_{\rm flow} = \Omega r^2$ as a function of the radius; as a comparison, we also show the Keplerian angular momentum in the same figure. Panel (d): variations in the density of the flow ρ. These solutions are drawn for different values of s, $s = 0$ (black), $s = 0.2$ (blue), and $s = 0.4$ (red). The vertical dashed line and the vertical dotted line correspond to the location of the marginally stable orbit (ISCO) and the Bondi radius $r_{\rm B}$, respectively.

slowly rotating accretion flows without outflow. Generally, the mass accretion rate decreases everywhere in the flow in the presence of the outflow. It is shown that the mass accretion rate decreases toward the black hole, which is a power-law form at the outer region, while it is constant in the inner region of flow, close to the black hole. Due to strong gravity near the BH, the combined fluid centrifugal force and pressure gradient force cannot overcome gravity. On the basis of this argument, it has been suggested that there will be little mass loss in the inner regions; in other words, the matter can never cross the flow surface, which causes s to equal 0. As the exponent s increases, the mass accretion rate onto the black hole decreases. The color bar represents the temperature of the flow. The temperature of the accretion flow decreases with the increase in the mass-loss rate. This phenomenon is because, in the accretion flow, a fraction of the gravitational energy is tapped to accelerate the outflow. This reduces the heating of the flow (Li & Cao 2009).

Figure 4 shows the variation in the mass accretion rate as a function of the exponent s, for two values of η, which represents the importance of energy carried away by outflow. In addition, in this figure $l = 1$. The left panel represents the BH accretion rate as a function of the exponent s; the mass accretion rate decreases as the intensity of mass outflow (s) increases. The color bar shows the specific angular momentum that the black hole swallows. It is evident that as the outflow intensity increases, the specific angular momentum swallowed by the BH decreases slightly. The right panel shows the mass accretion rate in the outer boundary $\dot{M}_{\rm out}$ as a function of the exponent s. As the intensity of the mass outflow (s) increases, the mass accretion rate in the outer boundary increases. The

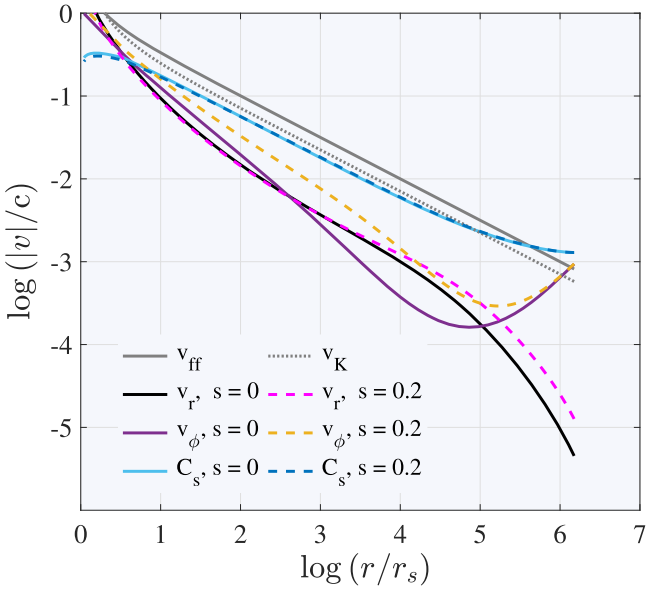

Figure 2. Various velocities of the accretion flow. The adiabatic index $\gamma = 5/3$ is adopted in the calculations. For comparison, the Keplerian velocity v_K and freefall velocity v_{ff} are plotted on top of the curves.

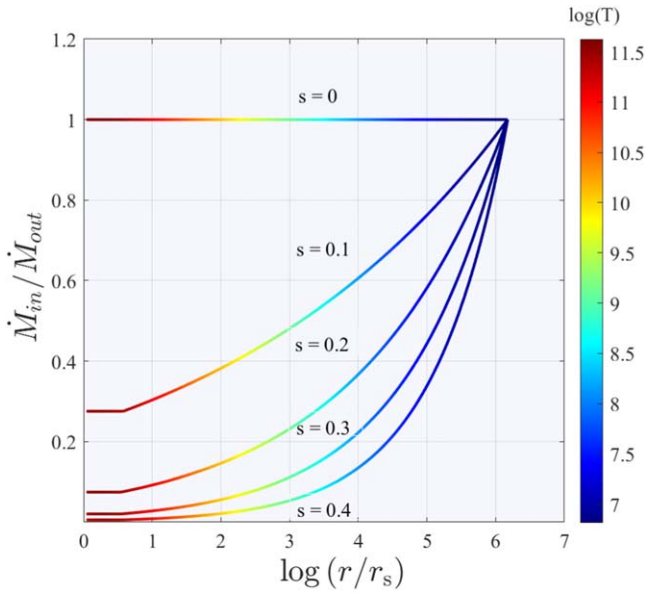

Figure 3. Mass accretion rate of the flow as a function of the radius, where $\dot{M}_{out}$ is the accretion rate at radius $r = r_{out}$. The colored lines indicate the results for different values of s. The top horizontal line shows the mass accretion rate without outflow ($s = 0$).

color bar shows the location of the sonic point. It can be well seen that the radius of the sonic point increases slightly as the outflow intensity (s) increases. When there is outflow, the mass accretion rates at the outer boundary are higher than those in the absence of outflow for the same gas conditions, including the gas angular momentum. The reason for this is that outflow removes angular momentum, so its presence leads to decreased gas angular momentum and, therefore, a higher mass accretion rate at the outer boundary (Park & Han 2018). Furthermore, as can be seen in the figure, the mass accretion rate increases by considering outflow cooling effects. In this figure, we see different $\dot{M}$ for two values of η parameter ($\eta = 1$ and $\eta = 0$). There is only minimal difference between when the outflow carries energy ($\eta = 1$) and when it does not ($\eta = 0$).

In the following, we tend to focus on the role of the dimensionless lever arm l. Figure 5 shows the variation in the mass accretion rate (left panel) and radial velocity (right panel) for different l. In the left panel, it is easily seen that the mass accretion rate onto the black hole is greater for $l = 2$ than $l = 0$. In the case of $l = 0$, the flow loses only mass, which corresponds to a nonrotating outflow. In the case of $l = 2$, the outflows carry away a considerable amount of the angular momentum of the flow and cause its structure to become significantly different from the conventional viscous flow structure. In the right panel, the radial velocity for $l = 2$ is larger than $l = 0$. Despite the fact that the radial velocity in the innermost region of the flow does not change due to the outflow, a rotating outflow increases the radial velocity in the outer region of the flow. According to this study, the radial velocity of an accretion flow in which the angular momentum is removed by the outflows is slightly higher than that of an accretion flow in which the angular momentum is not removed by outflows. In this panel, the color bar presents the pressure of the flow as a function of the radius. It was assumed that outflow material would rotate with the flow. The nonrotating outflow corresponds to $l = 0$. As l exceeds 0 ($l > 0$), the angular momentum is carried away by the outflow. In addition, outflows can remove more angular momentum from the flow, corresponding to $l > 1$, such as centrifugally driven magnetohydrodynamic winds (Blandford & Payne 1982; Wu et al. 2022).

Figure 6 represents the result of the solution for $s = 0.05$–0.5 and $L = 5 - 95$. Each panel of Figure 6 displays an image that uses the full range of colors in the color map. Each element specifies the color for one pixel of the image. The resulting image is a 19-by-19 grid of pixels (19 rows and 19 columns). The row and column indices of the elements determine the centers of the corresponding pixels. In each panel, the color bar shows the mass accretion rate. Areas with darker colors have lower mass accretion rates, and lighter colors have larger mass accretion rates. It is clear that the lower right region of each panel, which represents larger s values, i.e., stronger outflows, corresponds to disk-like outflows (larger L). In contrast, the upper left region in each panel represents smaller s values, i.e., weaker outflows, and corresponds to Bondi outflows (smaller L). According to the right-hand panel in Figure 6, $\dot{M}_{BH}$ decreases as the rotation of the external gas (L) increases. The left panel shows the variation in the mass accretion rate in the outer boundary as a function of parameters s and L. It is clear that by increasing s, the mass accretion rate in the outer boundary increases. The right panel shows the variation in the mass accretion rate in the black hole as a function of parameters s and L. It is clear that as the exponent s increases, the mass accretion rate onto the BH decreases, indicating that the outflow is removing mass.

The models in Table 1 are classified into two subclasses, i.e., models A1–A3 and B1–B3. Here, models A1–A3 are called A-type models, while models B1–B3 are called B-type models. The outer boundary of our calculation is $3r_B$ for the A-type models and r_B for the B-type models. Our numerical solutions with different outer boundaries are summarized in Table 1. Columns 2 and 3 of Table 1 show the temperature and angular momentum at the outer boundary, respectively. Columns 4–6 include the outflow parameters, s, η, and L, respectively.

Column 7 shows the location of the outer boundary in units of the Bondi radius, and column 8 shows the galaxy potential.

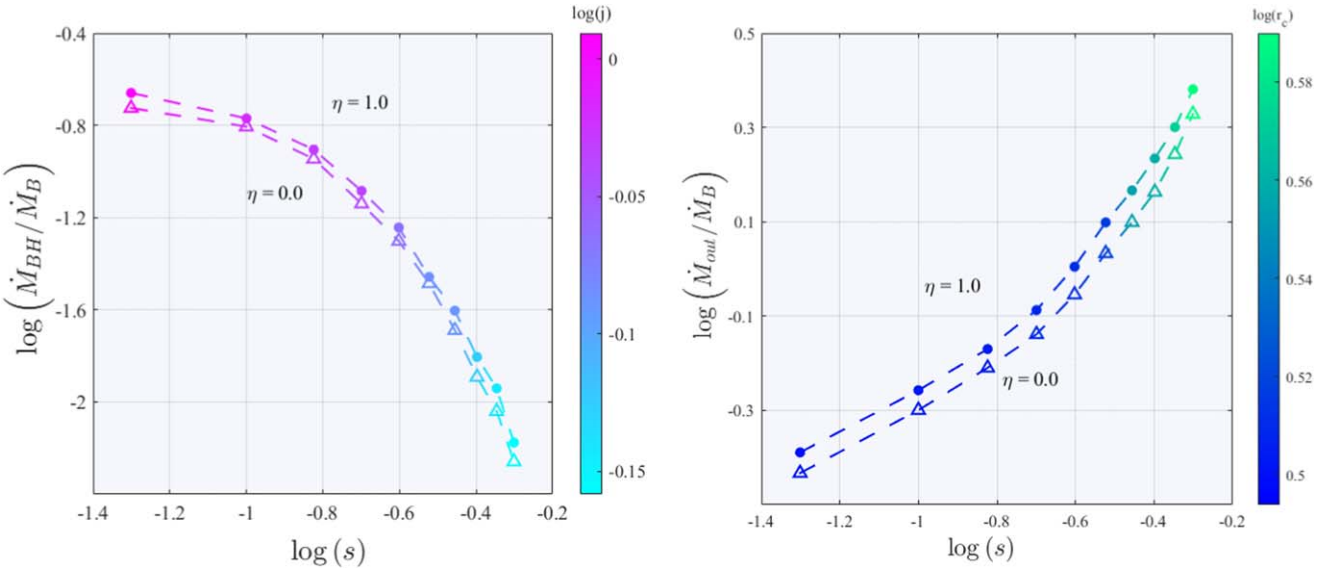

Figure 4. Left panel: mass accretion rate onto a BH as a function of the exponent s for different values of η, plotted for $L = 85$, $l = 1$ $\alpha = 0.1$, $\gamma = 5/3$, and $T_{\rm out} = 6.5 \times 10^6$ K. The color bar shows the specific angular momentum that is swallowed by the black hole. Right panel: mass accretion rate at the outer boundary as a function of the exponent s. The color bar shows the location of the sonic point.

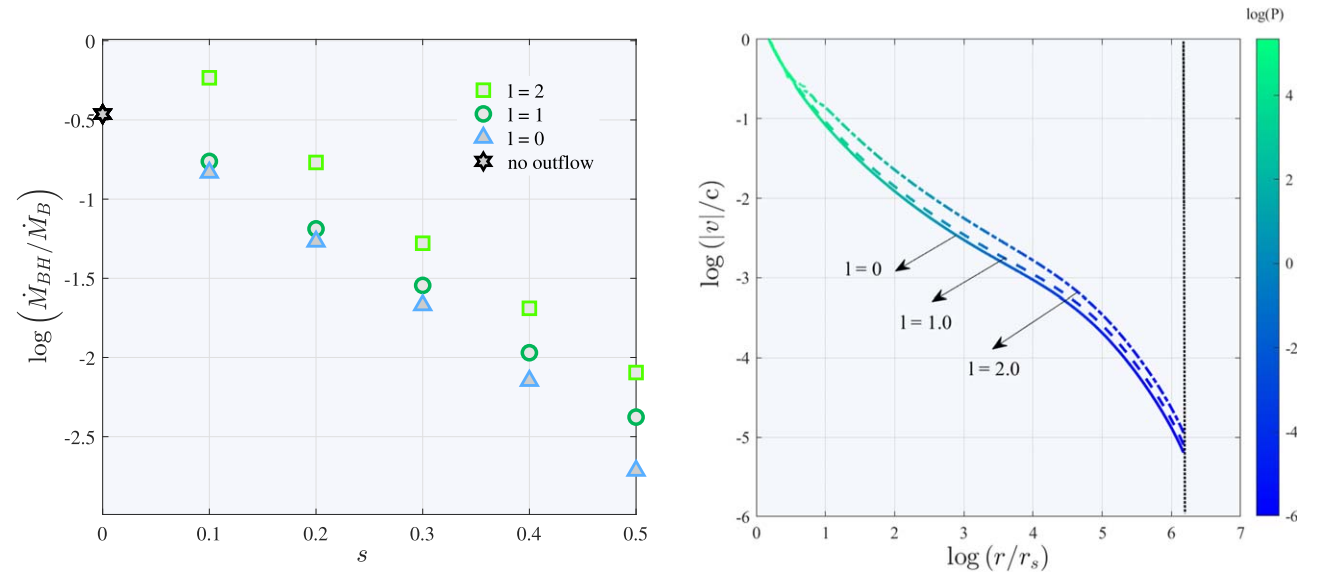

Figure 5. The left panel shows the mass accretion rate onto the black hole in units of the Bondi rate as a function of parameter s. The light green square, the dark green circle, and the blue triangles represent the mass accretion rates onto the black hole for $l = 2$, $l = 1$, and $l = 0$, respectively. The black hexagram shows the value of the mass accretion rate in the absence of outflows. The adiabatic index $\gamma = 5/3$ is adopted in the calculations. The right panel shows the variation in the radial velocity for three solutions $l = 2$, $l = 1$, and $l = 0$. The color bar shows the pressure of an accretion flow.

Columns 9 and 10 show the mass accretion rate onto BH and at the outer boundary in units of the Eddington accretion rate, respectively. We compare models with different outer boundary conditions, i.e., models A1, A2, and B1, B2, and give the results in Table 1. The results show that both the exponent s and specific angular momentum at the outer boundary L in model A2 have higher values than those model A1, while the BH accretion rate of model A2 is smaller than that of model A1. In models B1 and B2, the temperatures at the outer boundary are larger than those in models A1 and A2, and the BH accretion rates are smaller. Also, we compare the solutions of models A2 and A3. Model A2 includes the galaxy potential, while model A3 does not include it. It can be seen in Table 1 that the galaxy potential slightly increases the BH accretion rate, as had been achieved in our previous paper (R22). The same result can be obtained from the comparison of the B1 and B2 models. In essence, the present results show that galactic potential may play a significant role in the dynamics of the slowly rotating accretion flows and their outflows in massive ellipticals. Therefore, it is important not to overlook the galactic potential when modeling realistic (numerical and analytical) accretion dynamics. As a result, this would provide a better understanding of the energy of AGN feedback in the context of these massive galaxies in the contemporary universe.

3.1. Comparison with Previous Works

The purpose of this section is to compare the results with the simulation performed by Bu & Yang (2019; hereafter BY19) and the solution presented in our previous paper (R22). In order to

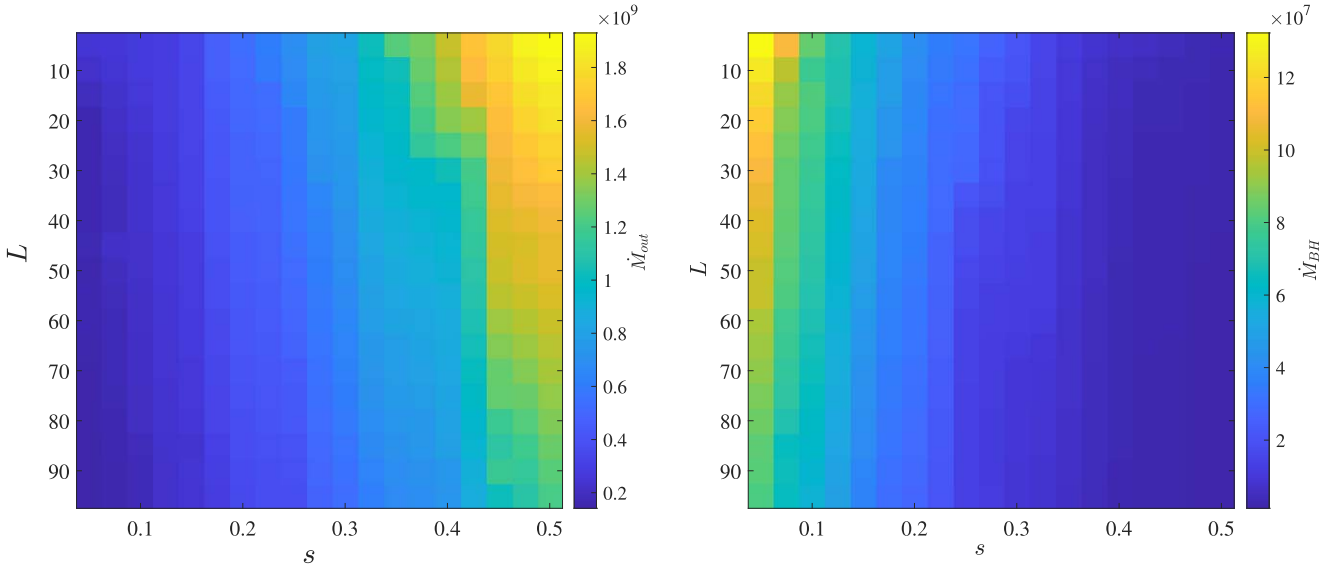

Figure 6. Mass accretion rate as a function of parameters s and L. Left panel: mass accretion rate in the outer boundary $\dot{M}_{\rm out}$. Right panel: Mass accretion rate onto the black hole $\dot{M}_{\rm BH}$. In each panel, the horizontal axis displays the strength of the outflow, the vertical axis shows the angular momentum at the outer boundary, and the color bar represents the mass accretion rate. The darker shaded areas have lower mass accretion rates, and the lighter colors have larger mass accretion rates.

Table 1
Summary of Our Model

Model ID	$T_{\rm out}$ (k)	L	s	η	l	$r_{\rm out}$ ($r_{\rm B}$)	$\phi_{\rm galaxy}$	$\dot{M}_{\rm BH}$ ($\dot{M}_{\rm Edd}$)	$\dot{M}_{\rm out}$ ($\dot{M}_{\rm Edd}$)
A1	3.9×10^6	5	0.2	1	1	3	ON	1.11×10^{-5}	1.62×10^{-4}
A2	3.9×10^6	85	0.5	1	1	3	ON	6.73×10^{-7}	5.68×10^{-4}
A3	3.9×10^6	85	0.5	1	1	3	OFF	4.46×10^{-7}	3.76×10^{-4}
B1	6.5×10^6	5	0.2	1	1	1	ON	7.64×10^{-6}	8.10×10^{-5}
B2	6.5×10^6	85	0.5	1	1	1	ON	4.89×10^{-7}	1.7×10^{-4}
B3	6.5×10^6	85	0.2	1	1	1	OFF	3.48×10^{-7}	1.32×10^{-4}

Note. Column (2) is the temperature at the outer boundary; column (3) is the angular momentum at the outer boundary, columns 4–6 are the parameters of the outflow; column (7) shows the location of the outer boundary; column (8) is the galaxy potential; and columns (9) and (10) are the mass accretion rate at the black hole and the outer boundary, respectively.

properly compare our model with these works, we consider the black hole mass equal to $10^8 M_\odot$ ($M_\odot$ is the solar mass) and the density at the outer boundary $\rho_0 = 10^{-24}$ gr cm^{-3}. Figure 7 shows the mass accretion rate of the black hole in units of $\dot{M}_E$ as a function of the temperature at the outer boundary. The dashed line shows the Bondi accretion rate by assuming $\gamma = 5/3$. We present our numerical solutions for three different values of the exponent s. The blue circles show our numerical solution without considering the outflow that corresponds to $s = 0$. The pink diamonds are our solution when $s = 0.1$. Solutions with $s = 0.3$ can be seen as green squares. The orange squares are according to the time-averaged values of the mass accretion rate of simulations in BY19, and the error bars on squares correspond to the change range of simulations due to fluctuations. The solid blue line is from the fitting formula (Equation (5) of BY19). The fitting formula is an analytical formula that can accurately predict the luminosity of observed LLAGNs (with black hole masses of $\sim 10^8 M_\odot$). The black hole accretion rate is calculated using this formula based on the density and temperature of the gas at the parsec scale. It is clear that the BH accretion rates of solutions without outflows are larger than those of other solutions. It has been shown that outflows can reduce the mass accretion rate onto the black hole. We find that the solution corresponding to $s = 0.3$ can represent the fitting formula well. Furthermore, we mention that they considered $s = 0.5$. Compared with YB19 simulations, our results deviate slightly due to ignoring radiation effects. Perhaps it is because our results agree with the simulation results at $s = 0.3$.

In the last step, by keeping the assumption of vertical hydrostatic equilibrium similar to our previous work (R22), we investigate the effect of an outflow on the thickness of the flow. In this part, we assume the initial state $H \neq r$ rather than the simple approximation $H = r$. Figure 8 indicates the radial variation in the relative thickness H/r of the flow in the presence of an outflow for various values of the exponent $s = 0$, 0.2, 0.4. The color bar shows the density of the accretion flow. It has been demonstrated that a flow without an outflow is thicker than a flow in the presence of an outflow. It has also been shown that outflows reduce the thickness of a flow. In other words, the thickness of a flow increases as the intensity of the outflow decreases. As is evident from the results, at intermediate radii, such as (10–10^5) $r_{\rm s}$, the flow thickness H/r

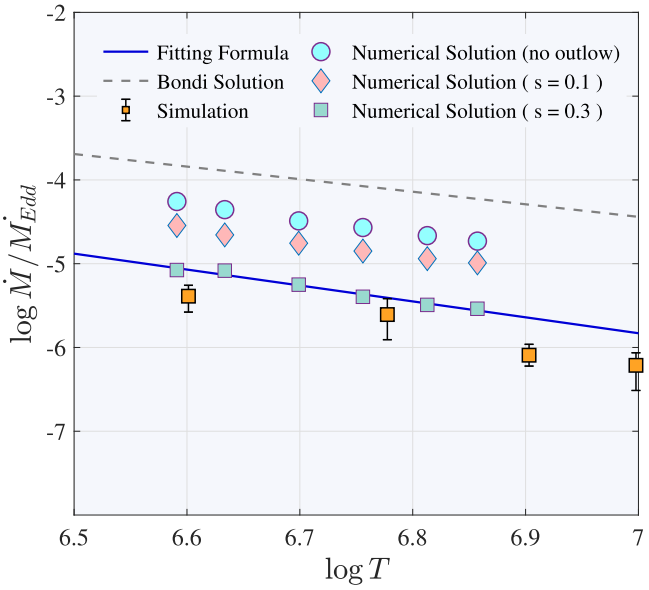

Figure 7. Mass accretion rate of the black hole in units of $\dot{M}_E$ as a function of the temperature at the outer boundary $T_{\rm out}$. The density at the outer boundary is considered $\rho_0 = 10^{-24}{\rm gr/cm^3}$. Solutions are for $L = 85$, $\alpha = 0.1$, $r_{\rm out} = 3r_B$, and $\gamma = 5/3$.

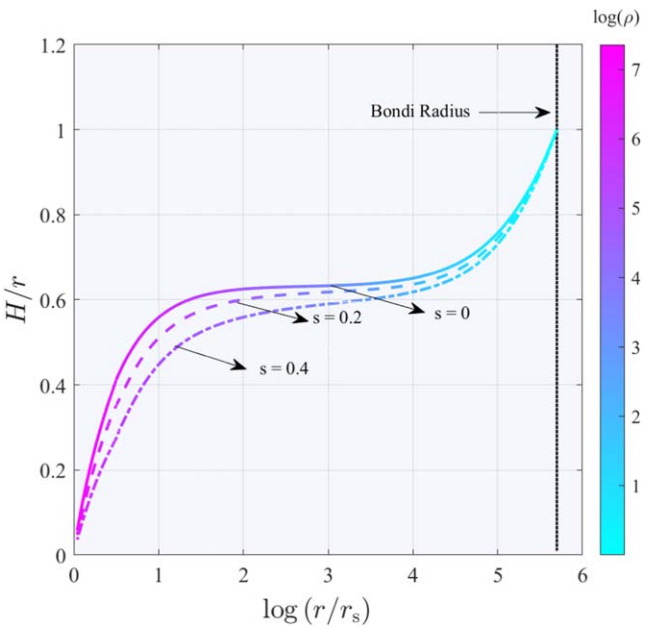

Figure 8. Radial variation in the relative thickness of the flow H/r for $s = 0$, $s = 0.2$, and 0.4. The vertical dotted line indicates the location of the Bondi radius. The solutions are for $L = 85$, $\alpha = 0.1$, $\gamma = 5/3$ and $T_{\rm out} = 6.5 \times 10^6$ K, $\eta = 1$, $r_{\rm out} = r_B$. The color bar shows the density of the accretion flow.

can vary between 0.4 to 0.6 for different s (0.4–0). According to our results, accretion flows with stronger outflows will be thinner than those without outflows. In this part, the outer boundary is fixed to the Bondi radius $r_{\rm out} = r_{\rm B}$, similar to our previous work (R22).

3.2. Mechanical AGN Feedback

In this section, we discuss in detail how the properties of an outflow are calculated for a given accretion rate. We want to know, for a given accretion rate, what will be the output of an AGN, or what will the wind properties be? In our accretion mode, an accretion flow produces an outflow but not radiation or a jet. It is assumed that jets deposit very little energy in the galaxy, so we neglect them here. In the future, this assumption needs to be examined. As the wind is launched from the accretion flow, it will affect the black hole's accretion rate. A fraction of the gas in the accretion flow is ejected in the form of wind. So the outflow mass flux can be obtained from Equation (5).

As a result, the accretion rate close to the horizon of a black hole, which determines its luminosity, is described by the following equation:

$$\dot{M}_{\rm BH} = \dot{M}_{\rm out}\left(\frac{r_{\rm c}}{r_{\rm out}}\right)^s. \tag{25}$$

Similar to Yuan et al.'s (2018) work, we assume $s = 0.5$ in this section. The opening angle of the outflow is greater than that of jets, which makes the interaction between the wind and the ISM more efficient (refer to Figure 1 in Yuan et al. 2015). According to previous investigations (Yuan et al. 2015, Equation (8)), an outflow's poloidal velocity roughly remains constant and is approximated as follows:

$$v_{\rm w} = (0.2 - 0.4)v_{\rm k}(r_{\rm out}). \tag{26}$$

Here $v_{\rm k}$ is the Keplerian velocity at the outer radius $r_{\rm out}$.

Here we assume $v_w = 0.2v_k(r_{\rm out})$ and consequently the flux of the energy and momentum of the outflow will be introduced as:

$$\dot{E}_w = \frac{1}{2}\dot{M}_w v_k^2, \tag{27}$$

$$\dot{P}_w = \frac{2\dot{E}_w}{v_w}. \tag{28}$$

By comparing the energy and momentum fluxes of the wind in the cold and hot feedback modes with those produced by our model, we are able to evaluate the validity of our parametric model. The results of such a comparison are shown in Figure 9. The left and right panels denote the power and momentum fluxes, respectively. In both hot and cold modes, the wind momentum flux is large, suggesting that outflow will be instrumental in pushing gas away from an AGN. As a comparison between our current description of outflows and previous studies, we have also explored the AGN model from Gan et al. (2014). It can be seen from Figure 9 that slowly rotating accretion flows have lower black hole accretion rates than hot and cold modes (10^{-5}–$10^{-7}\dot{M}_{\rm Edd}$). Here, $\dot{M}_{\rm Edd} = 10L_{\rm Edd}/c^2$ is the Eddington accretion rate.

Also, the wind's energy and momentum flux are lower than those in the cold and hot feedback modes. This means that the wind is less powerful in an accretion flow that rotates slowly. Depending on parameter s, the wind power ranges from 10^{-10}–$10^{-12}L_{\rm Edd}$ and the momentum flux of the wind ranges from 10^{28}–10^{30} grcm s^{-2}. As parameter s increases, the energy and momentum fluxes of the wind slightly increase. In addition, we showed the solutions for two values of the angular momentum ($L = 85$ and $L = 5$) at the outer boundary. As we can see, the power and momentum fluxes are not much different in both these modes. We should not judge which is important in the feedback simply from its magnitude of power and momentum flux. Due to the different cross sections of photon–particle and particle–particle interactions, the outflow

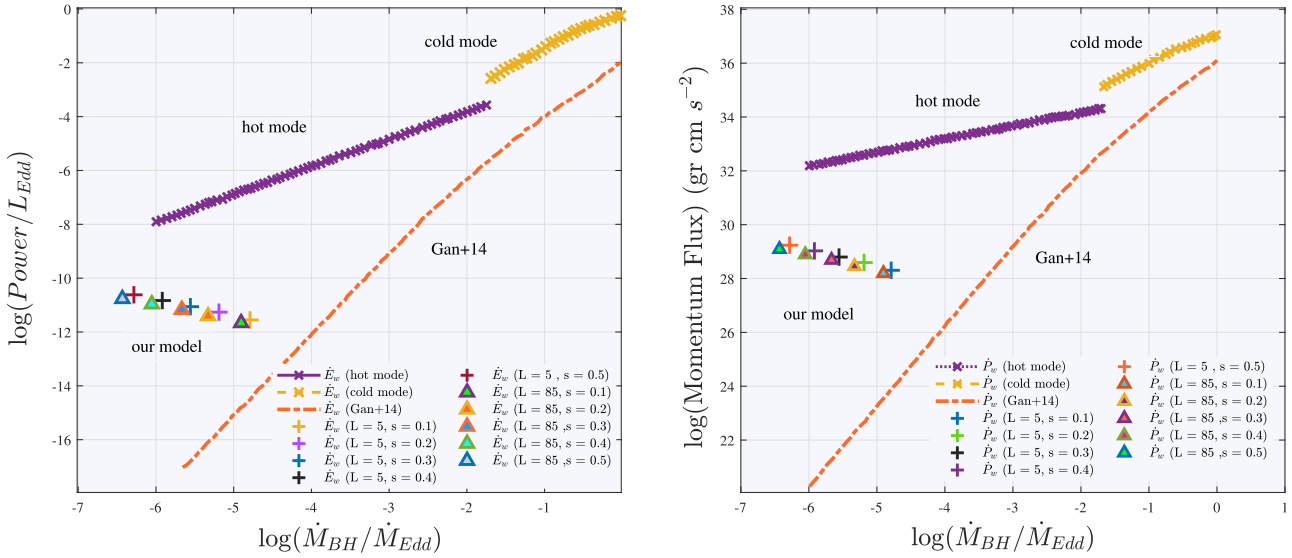

Figure 9. For $L = 85$, $\alpha = 0.1$, $\gamma = 5/3$ and $T_{\rm out} = 6.5 \times 10^6$ K, $\eta = 1$,. The comparison of the power (left) and momentum flux (right) of the outflow in the hot (Violet lines) and cold (Orange lines) accretion modes of AGNs with our model. As a comparison, the red dotted–dashed lines show the wind's power and momentum flux from Gan et al. (2014).

must travel very different distances to convert its energy and momentum to the ISM. In this study, we ignore the effects of mechanical AGN feedback on the cosmological formation of elliptical galaxies and black hole growth.

4. Discussion and Summary

Outflows play a significant role in the active galactic nuclei feedback process. The aim of this paper is to investigate the influence of outflows on the structure and physical properties of slowly rotating accretion flows. Pioneer works of numerical simulation of black hole accretion flows have found that the mass accretion rate decreases inward. It can be seen that hydrodynamic winds, that is, outflows, help maintain the accretion process by carrying mass, energy, and angular momentum away. The gas angular momentum or outflow could lead to a decrease in the mass accretion rate, which will profoundly affect the growth of SMBHs and their coevolution with host galaxies. The outflows from the central engine are tightly coupled with the surrounding gaseous medium, providing the dominant heat source and preventing runaway cooling. This study does not consider the interaction between the outflow and its surrounding environment. According to many previous studies, the outflow is induced by assuming the mass accretion rate $\dot{M}$ to be a power-law function of the radius, $\dot{M} \propto r^s$ (e.g., Blandford & Begelman 1999). So based on the assumption that the outflow mass-loss rate follows a power-law distribution in radius, the calculations were simplified. The parametric approach used in the present study can be applied to a wide range of dynamical outflow models, including radiation-driven and centrifugally driven outflows. Similar to our previous work, a transition from subsonic to supersonic occurs as matter moves inward with increasing radial velocity along the radial direction. Our study assumes that the mass accretion rate $\dot{M}$ decreases toward the black hole, which has a power-law r-dependence at larger radii but is constant in the inner region of the flow close to the black hole. For $r \leqslant 10 r_{\rm s}$, we considered only the inflow region, and the flow is supersonic.

We find that in the presence of an outflow, the structure of a slightly rotating accretion flow is significantly altered. The outer boundary is usually located at several hundred or thousands of Schwarzschild radius ($\sim 3 r_B \sim 10^6 r_{\rm s}$). The effect of radiative cooling on the outflow strength has not been discussed in this paper.

To be more precise, this model has modified the classical Bondi model, and the angular momentum of the gas is very small. The potential energy of the black hole, as well as the host galaxy, is taken into account. The main results of this work are briefly described below.

1. The mass accretion rates of slowly rotating accretion flows with outflows are no longer constant radially. It was observed in our model that the radial density profile is flatter because the mass accretion rate decreases with decreasing radius. Basically, if the mass accretion rate were constant with the radius, the density profiles would be steeper.
2. It was found that the radial velocity of the flow with winds at the outer edge of the accretion flow is significantly higher than that of a conventional accretion flow.
3. Based on our results, the flow thickness decreases as the outflow intensity increases.
4. Owing to the galactic contribution to the potential, there is an enhancement in the value of the mass accretion rate relative to the initial case, and the galactic contribution to the potential has a significant effect on the velocity profile.
5. The mass accretion rate onto the BH in our solutions is in good agreement with the formula obtained in YB19, which is based on the density and temperature of the gas at the parsec scale. This formula accurately predicts the luminosity of LLAGNs (with black hole masses of $\sim 10^8 M_\odot$).
6. The energy and momentum fluxes of the outflow in our model are less than those in the cold and hot feedback modes. AGN feedback in slowly rotating accretion flows probably has less impact on the surrounding environment due to weak outflows.

The solutions we have developed and the flow structure differ from those in previous analytical studies in many aspects (e.g., boundary conditions, the behavior of solutions, and the subsonic region). Outflows can very effectively affect the properties of the gas surrounding AGNs (Yuan et al. 2018). There is also evidence that wind/outflow can suppress star formation more strongly than radiation.

In this study, we have not taken the interaction between winds and the ISM into account. We plan to pursue this interaction in our future work.

Acknowledgments

We hereby acknowledge the Sci-HPC center of the Ferdowsi University of Mashhad where some of this research was performed. Also, we have made extensive use of the NASA Astrophysical Data System Abstract Service. This work was supported by the Ferdowsi University of Mashhad under grant No. 57030 (1400/11/02).

ORCID iDs

Razieh Ranjbar https://orcid.org/0000-0003-1488-4890
Shahram Abbassi https://orcid.org/0000-0003-0428-2140

References

Abbassi, S., Ghanbari, J., & Ghasemnezhad, M. 2010, MNRAS, 409, 1113
Abbassi, S., Nourbakhsh, E., & Shadmehri, M. 2013, ApJ, 765, 96
Baganoff, F. K., Maeda, Y., Morris, M., et al. 2003, ApJ, 591, 891
Bai, X. N., & Stone, J. M. 2013, ApJ, 767, 30
Begelman, M. C. 2012, MNRAS, 420, 2912
Blandford, R. D., & Begelman, M. C. 1999, MNRAS Lett., 303, L1
Blandford, R. D., & Payne, D. G. 1982, MNRAS, 199, 883
Bondi, H. 1952, MNRAS, 112, 195
Botella, I., Mineshige, S., Kitaki, T., Ohsuga, K., & Kawashima, T. 2022, PASJ, 74, 384
Bu, D.-F., & Yang, X.-H. 2019, ApJ, 882, 55
Bu, D. F., & Yang, X. H. 2019, MNRAS, 484, 1724
Bu, D. F., Yuan, F., Wu, M., & Cuadra, J. 2013, MNRAS, 434, 1692
Bu, D.-F., Yuan, F., Gan, Z.-M., & Yang, X.-H. 2016, ApJ, 818, 83
Cao, X., & Spruit, H. C. 2002, A&A, 385, 289
Chakrabarti, S. K. 1996, ApJ, 464, 664
Cheung, E., Bundy, K., Cappellari, M., et al. 2016, Natur, 533, 504
Ciotti, L., Ostriker, J. P., & Proga, D. 2010, ApJ, 717, 708
Ciotti, L., & Pellegrini, S. 2017, ApJ, 848, 29
Ciotti, L., & Pellegrini, S. 2018, ApJ, 868, 91
Ciotti, L., Pellegrini, S., Negri, A., & Ostriker, J. P. 2017, ApJ, 835, 15
Crenshaw, D. M., & Kraemer, S. B. 2012, ApJ, 753, 11
Czerny, B., Moscibrodzka, M., Proga, D., Das, T. K., & Siemiginowska, A. 2007, in Proc. of RAGtime 8/9: Workshops on Black Holes and Neutron Stars, ed. S. Hledík & Z. Stuchlík, 35
Di Matteo, T., Allen, S. W., Fabian, A. C., Wilson, A. S., & Young, A. J. 2003, ApJ, 582, 133
Di Matteo, T., Quataert, E., Allen, S. W., et al. 2000, MNRAS, 311, 507
Fabian, A. C. 2012, ARA&A, 50, 455
Frank, J., King, A., & Raine, D. 2002, Accretion power in astrophysics. (Cambridge: Cambridge Univ. Press)
Gan, Z., Yuan, F., Ostriker, J. P., Ciotti, L., & Novak, G. S. 2014, ApJ, 789, 150
Ghasemnezhad, M., & Abbassi, S. 2016, MNRAS, 456, 71
Habibi, A., & Abbassi, S. 2019, ApJ, 887, 256
Harrison, C. M., Costa, T., Tadhunter, C. N., et al. 2018, NatAs, 2, 198
Homan, J., Neilsen, J., Allen, J. L., et al. 2016, ApJL, 830, L5
Hu, Y., Federrath, C., Xu, S., & Mathew, S. S. 2022, MNRAS, 513, 2100
Igumenshchev, I. V., & Abramowicz, M. A. 1999, MNRAS, 303, 309
Igumenshchev, I. V., Abramowicz, M. A., & Narayan, R. 2000, ApJL, 537, L27
King, A., & Pounds, K. 2015, ARA&A, 53, 115
Knigge, C. 1999, MNRAS, 309, 409, (K99)
Kormendy, J., & Luis, C. H. 2013, ARA&A, 51, 511
Korol, V., Ciotti, L., & Pellegrini, S. 2016, MNRAS, 460, 1188
Kumar, R., & Gu, W. M. 2018, ApJ, 860, 114
Li, J., Ostriker, J., & Sunyaev, R. 2013, ApJ, 767, 105
Li, S.-L., & Cao, X. 2009, MNRAS, 400, 1734
Lubow, S. H., Papaloizou, J. C. B., & Pringle, J. E. 1994, MNRAS, 268, 1010
Lucchini, M., Krauß, F., & Markoff, S. 2019, MNRAS, 489, 1633
Ma, R.-Y., Roberts, S. R., Li, Y.-P., & Wang, Q. D. 2019, MNRAS, 483, 5614
McKinney, J. C., Tchekhovskoy, A., & Blandford, R. D. 2012, MNRAS, 423, 3083
Mosallanezhad, A., Abbassi, S., & Beiranvand, N. 2014, MNRAS, 437, 3112
Mukhopadhyay, B., & Ghosh, S. 2003, MNRAS, 342, 274
Muñoz-Darias, T., Jiménez-Ibarra, F., Panizo-Espinar, G., et al. 2019, ApJL, 879, L4
Narayan, R., & Fabian, A. C. 2011, MNRAS, 415, 3721
Narayan, R., Kato, S., & Honma, F. 1997, ApJ, 476, 49
Narayan, R., Sądowski, A., Penna, R. F., & Kulkarni, A. K. 2012, MNRAS, 426, 3241
Narayan, R., & Yi, I. 1994, ApJL, 428, L13
Ohsuga, K., Mori, M., Nakamoto, T., & Mineshige, S. 2005, ApJ, 628, 368
Ostriker, J. P., Choi, E., Ciotti, L., Novak, G. S., & Proga, D. 2010, ApJ, 722, 642
Paczynsky, B., & Wiita, P. J. 1980, A&A, 88, 23
Park, M.-G., & Han, D.-H. 2018, in EPJ Web of Conf. 168, ed. B. Gwak et al. (Seoul: EDP Sciences)
Proga, D., & Begelman, M. C. 2003, ApJ, 582, 69
Ranjbar, R., Mosallanezhad, A., & Abbassi, S. 2022, MNRAS, 516, 3984, (R22)
Roshan, M., & Abbassi, S. 2014, PhRvD, 90, 044010
Sądowski, A., Narayan, R., Penna, R., & Zhu, Y. 2013, MNRAS, 436, 3856
Samadi, M., & Abbassi, S. 2016, MNRAS, 455, 3381
Samadi, M., Zanganeh, S., & Abbassi, S. 2019, MNRAS, 489, 3870
Shakura, N. I., & Sunyaev, R. A 1973, A&A, 24, 337
Stone, J. M., Pringle, J. E., & Begelman, M. C. 1999, MNRAS, 310, 1002
Wang, Q. D., Nowak, M. A., Markoff, S. B., et al. 2013, Sci, 341, 981
Weinberger, R., Springel, V., Hernquist, L., et al. 2016, MNRAS, 465, 3291
Wong, K.-W., Irwin, J. A., Yukita, M., et al. 2011, ApJL, 736, L23
Wu, W.-B., Gu, W.-M., & Sun, M. 2022, ApJ, 930, 10
Yang, X. H., & Bu, D.-F. 2018, MNRAS, 478, 2887
Yuan, F., & Bu, D.-F. 2010, MNRAS, 408, 1051
Yuan, F., Bu, D., & Wu, M. 2012, ApJ, 761, 130
Yuan, F., Gan, Z., Narayan, R., et al. 2015, ApJ, 804, 101
Yuan, F., Markoff, S., & Falcke, H. 2002, A&A, 383, 854
Yuan, F., & Narayan, R. 2014, ARA&A, 52, 529
Yuan, F., Quataert, E., & Narayan, R. 2003, ApJ, 598, 301
Yuan, F., Wu, M., & Bu, D. 2012, ApJ, 761, 129
Yuan, F., Yoon, D., Li, Y. P., et al. 2018, ApJ, 857, 121